

Supplemental Data for:

## Spectroscopic, Thermodynamic and Computational Evidence of the Locations of the FADs in the Nitrogen Fixation-Associated Electron Transfer Flavoprotein†

Nishya Mohamed-Raseek,<sup>a</sup> H. Diessel Duan,<sup>a</sup> Peter Hildebrandt,<sup>b</sup> Maria Andrea Mroginski<sup>b</sup> and Anne-Frances Miller<sup>\*a,b</sup>

Supplemental Table S1:

Chain	Substitution	Forward primer	Reverse Primer
S	T94A/T97A	5'-gcggcgagctacgcgctcgccgcc-3'	5'-cagcgcgctcggagccggcgaagaacc-3'
S	T94P/T97V	5'-gcgccgagctacgcgctcgccgcc-3'	5'-cagcgggctcggagccggcgaagaacc-3'
S	G127E	5'-acctgggcggtgtcttcgctgatggctgc-3'	5'-gcagaccatcgacgaagacaccgccaggt-3'
S	V232K	5'-gccgacggtgaaaaagcgcgtgttcg-3'	5'-gaaccgaggaggccgcac-3'
S	V232Y	5'-gccgacggtgtacaagcgcgtgttcgcac-3'	5'-gaaccgaggaggccgcac-3'
S	D93T	5'-cgccggctccaccacgctggcg-3'	5'-aagaaccgatcggtcagcag-3'
L	R165Q	5'-cgccgaaggtcggctgcgtcggcgag-3'	5'-ctcgccgcgacgcagccgaccttcggcg-3'
L	R165K	5'-tgaagtcgagaaacgctccgaaggcg-3'	5'-atggtgcgagcctcgagg-3'

Table S1: The mutants were made by creating mutations in both genes, *fixA* encoding EtfS, and *fixB* encoding EtfL. A *fixA* gene-bearing plasmid and a *fixB* gene bearing plasmid were co-transformed into *E. coli* to permit expression of variant ETFs. Doubly-substituted proteins could be produced by combining two mutated genes, while singly substituted ETF could be produced by combining one mutant *fix* gene with a WT one.

Supplemental Figure S1

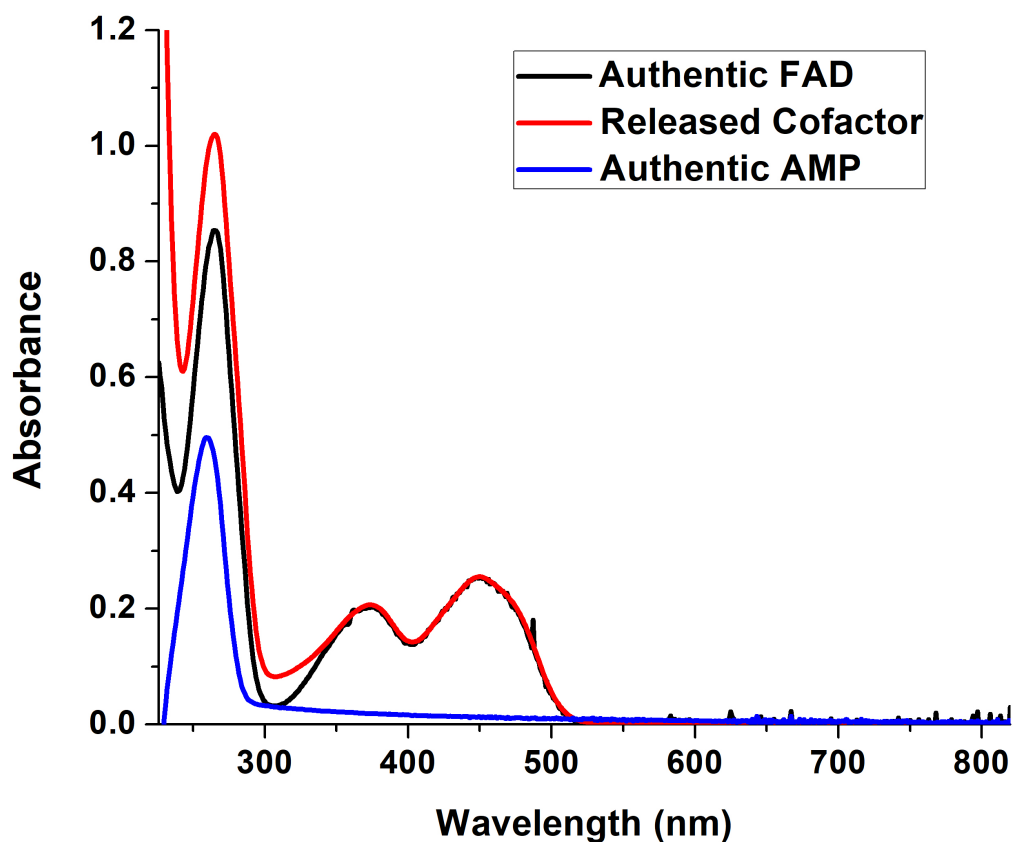


Figure S1: UV-Vis spectra of cofactors released from 28  $\mu\text{M}$  T94/97A ETF (black), authentic FAD (blue) and authentic AMP (red). The vertical scale of the authentic FAD spectrum was adjusted to mimic a concentration 23  $\mu\text{M}$  as for the released FAD spectrum, and the spectrum of authentic AMP was adjusted to concentration to reproduce a concentration of 33  $\mu\text{M}$  as for that of released AMP. These concentrations result from the finding of 0.8 FAD per ETF dimer and 1.2 AMP per ETF dimer.

Supplemental Figure S2

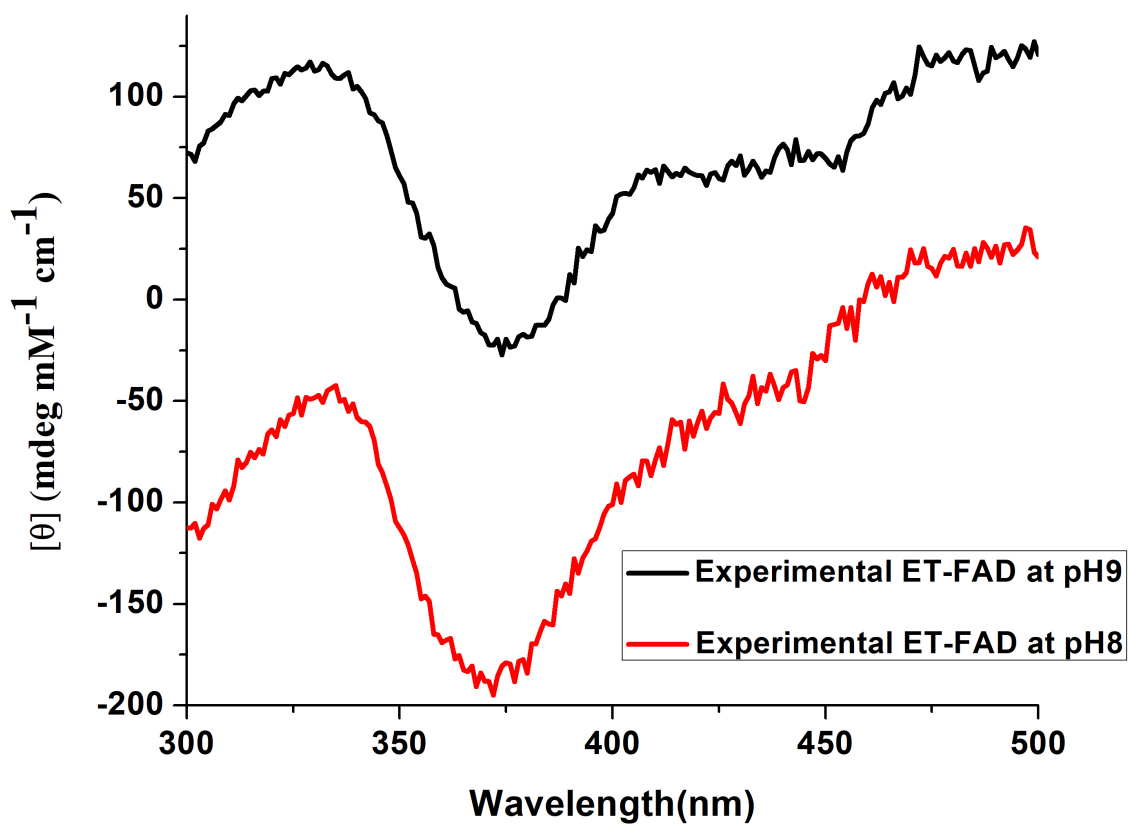


Figure S2: CD spectra of T94/97A ETF at pHs 8 and 9. Most of the data in this paper were collected at pH 8, in order to suppress formation of 8-formyl flavin. However corresponding data on WT *Rpa*ETF were collected at pH 9. Comparison of the visible CD spectra demonstrate that the flavin electronic structure of T94/97A ETF is not significantly different at pH 8 than at pH 9, so comparisons can be made between pH 8 T94/97A *Rpa*ETF and pH 9 WT *Rpa*ETF.

Supplemental Figure S3

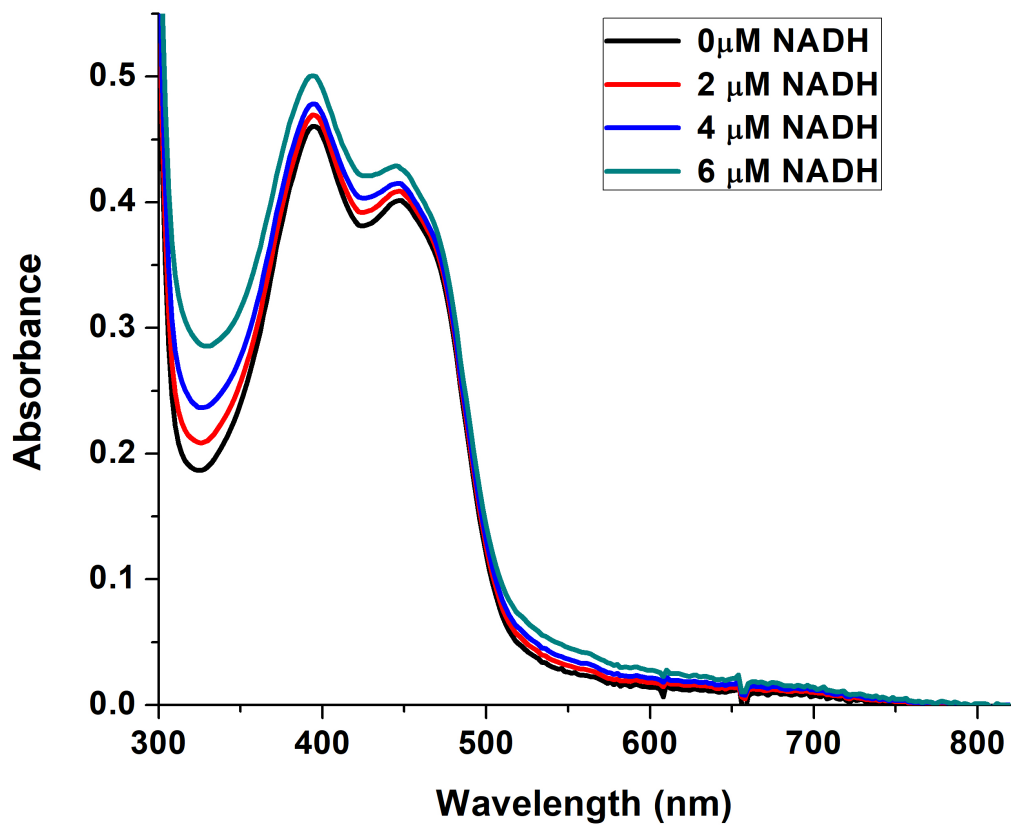


Figure S3: Visible spectra documenting the result of stepwise addition of NADH to 35 μM T94A/T97A ETF. The signature of oxidized flavin persisted despite accumulating NADH, but the protein began to aggregate at high [NADH] (note rising baseline, especially at short wavelengths).

## Supplemental Figure S4

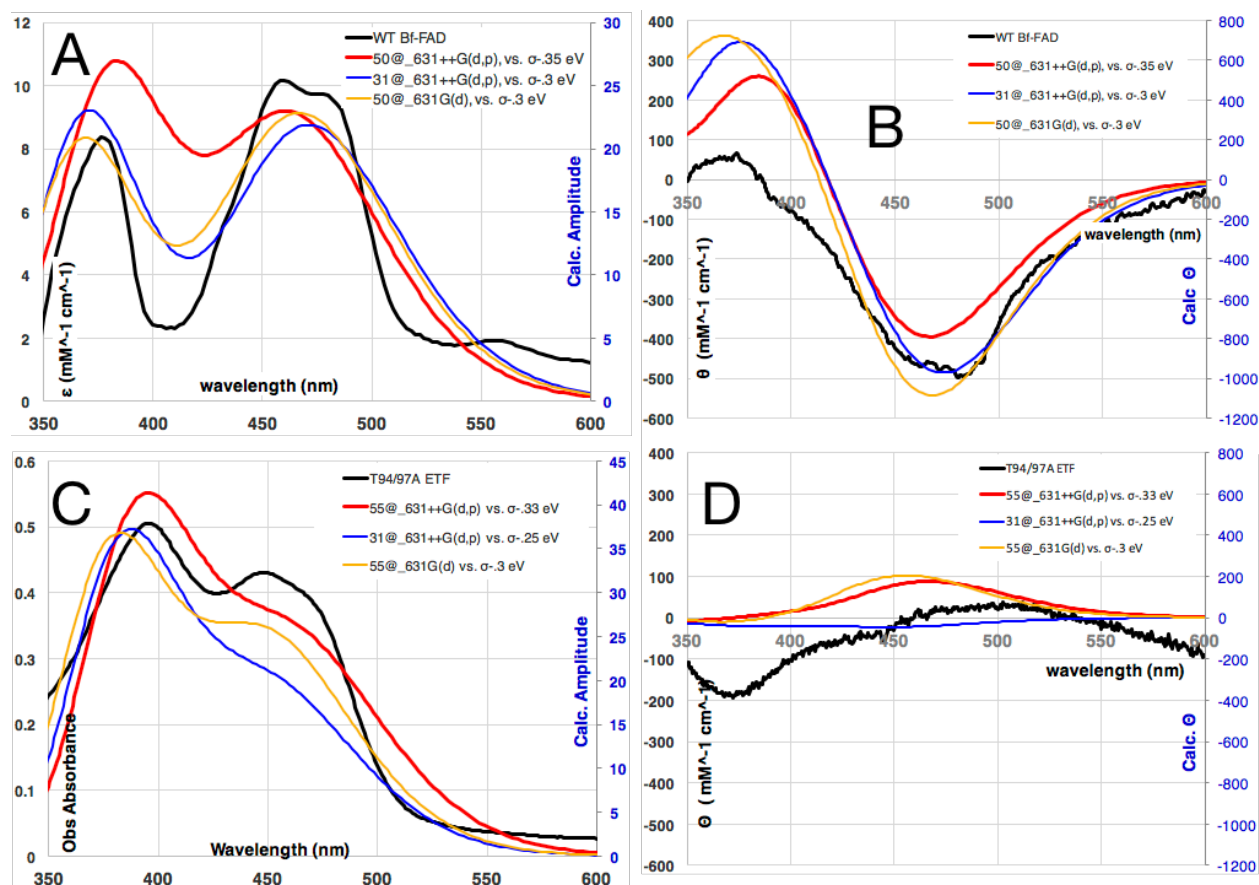


Figure S4: Comparison of the predictions obtained from the use of two sizes of quantum zone, and two sizes of basis set. Panels A and C show absorbance spectra while panels B and D show CD spectra. Panels A and B depict results for the domI/III site whilst panels C and D depict results for the domII site. Experimental spectra are in black. The smaller quantum zone treats only lumiflavin (yellow traces), in which the ribose is truncated at the C attached to the flavin, whereas the larger quantum zones (red and blue traces) also include atoms of a few nearby residues that hydrogen bond with the flavin or provide local charge (Supplemental Figure S5). The larger basis set (red and yellow traces) did a better job of reproducing the separation between the two lowest-energy bands. Supplemental Figure S9 reaches the same conclusion by considering ability to replicate the spectrum of FMN in neutral pH water.

Supplemental Figure S5

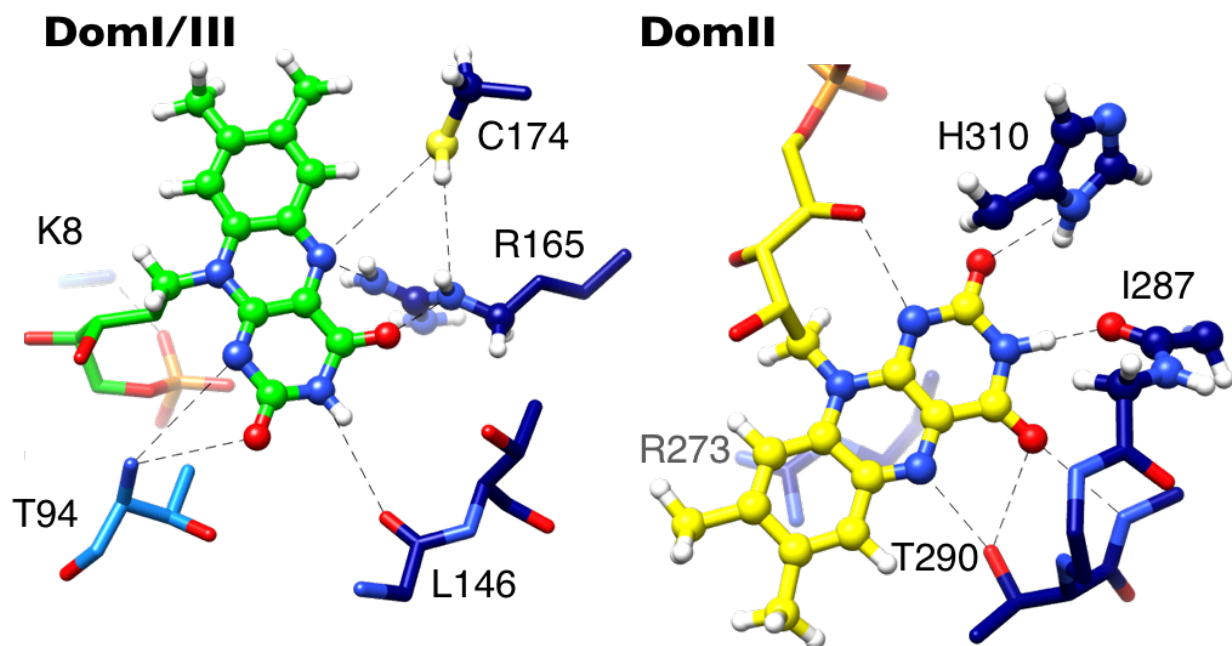


Figure S5: Atoms included in the 50-atom and 55-atom QM zones of the domain I/III flavin and domain II flavin, respectively, are depicted using ball&stick, additional atoms are depicted with sticks and H atoms are hidden. Residues from EtfL are in dark blue, whereas residues from EtfS are in light blue.

Supplemental Figure S6

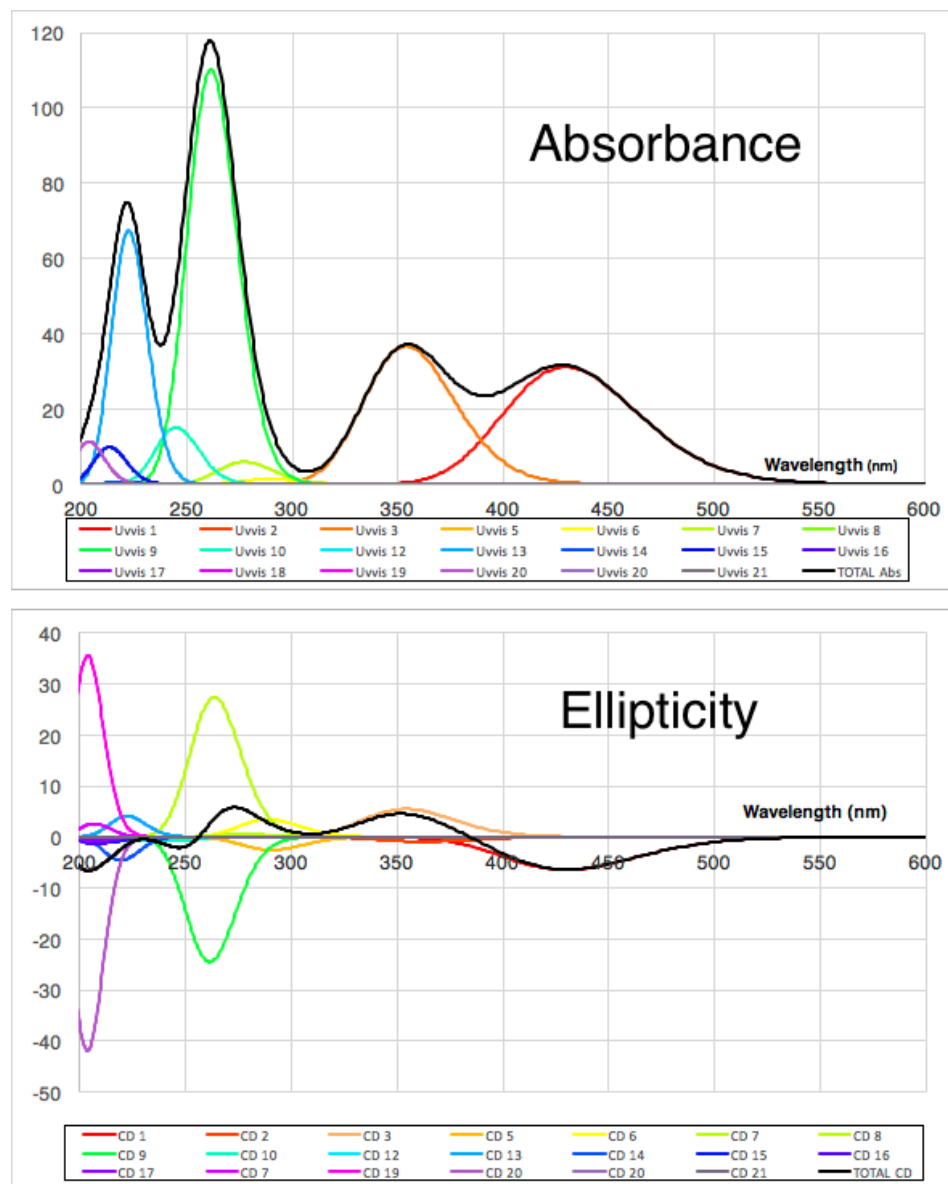
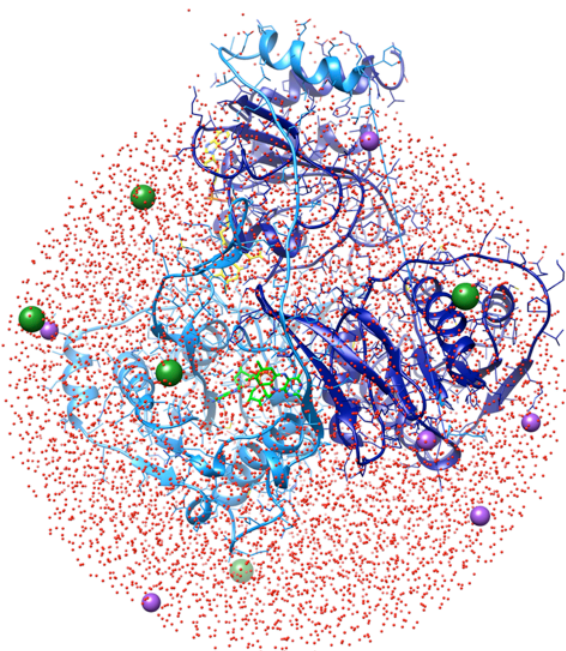


Figure S6: TD-DFT predictions for the optical absorbance and circular dichroism of free flavin in water, wherein lumiflavin was used as the model flavin (ribose is truncated at the C attached to the flavin) and water is modeled as self-consistent reaction field using continuous polarizable dipole model the 631++G(d,p) basis set and B3LYP functional were used, along with a Gaussian lines of 0.5 eV wide at half height, to calculate the observed spectrum (black) from the calculated transitions (coloured). For details of these and other calculated spectra please see the Methods.

Supplemental Figure S7

**DomI/III-FAD**



**DomII-FAD**

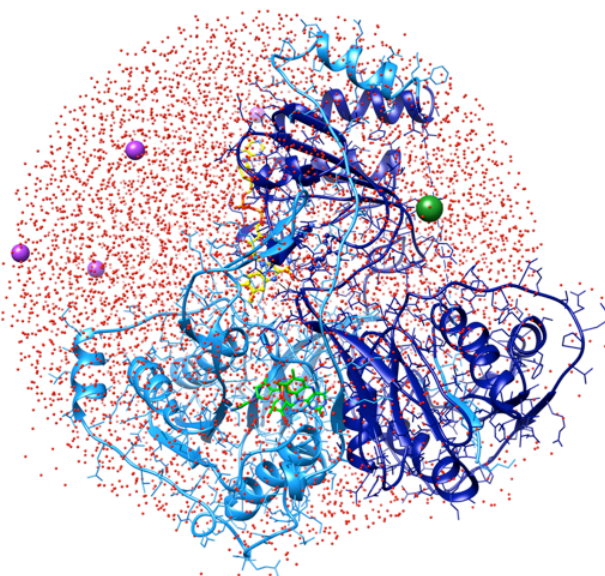


Figure S7: 40 Å spheres of TIP3 water and 100 mM ions ( $K^+$  and  $Cl^-$ ) retained after molecular dynamic equilibration, prior to QMMM treatments of the domain I/III flavin (left) or domain II flavin (right).

Supplemental Figure S8

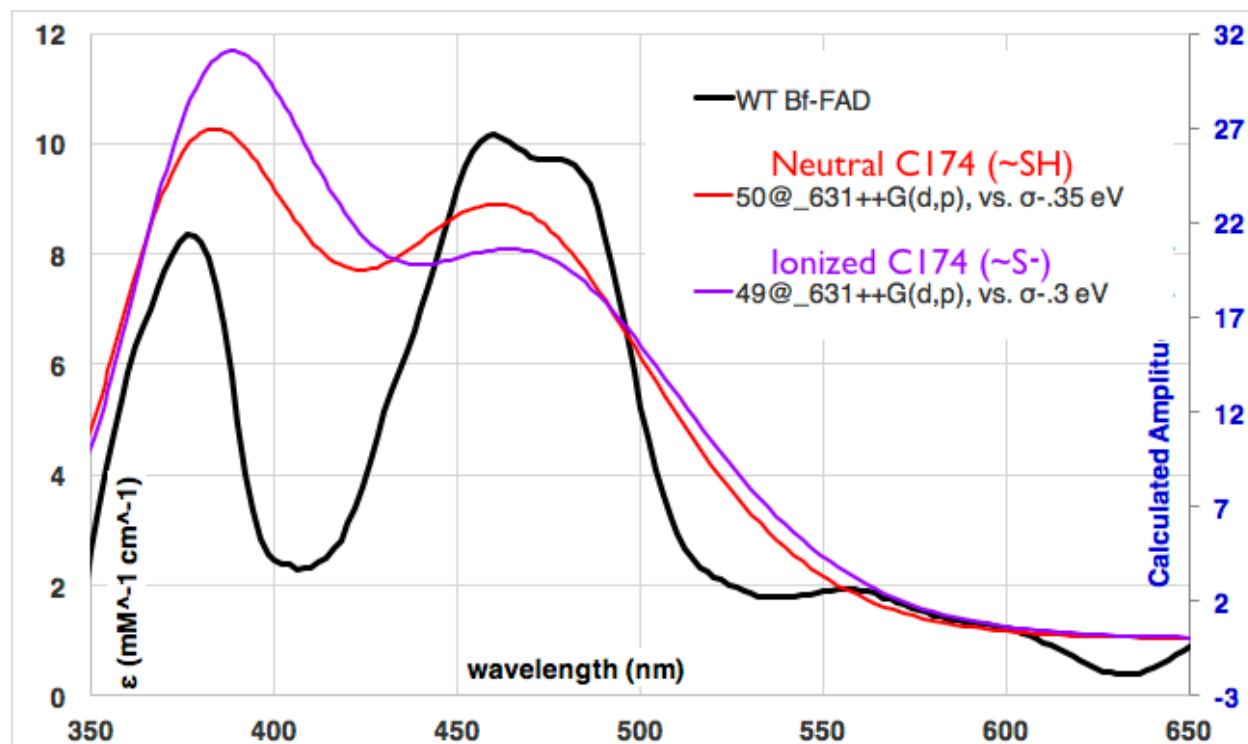


Figure S8: Comparison of absorbance spectra predicted for two plausible ionization states of the Cys 174 found near the domI/III-flavin. Both calculations employed the same computational protocol although separate MM optimizations were employed for the two different scenarios to account for the different charge distributions expected in response to different charges at Cys 174. The relative amplitudes of the two bands observed (black) agree better with those calculated assuming neutral Cys 174. Despite calculated absorbance resembling that of the domII flavin, the CD predicted in the presence of ionized Cys 174 remains in agreement with the domI/III site, not the domII site.

Supplemental Figure S9

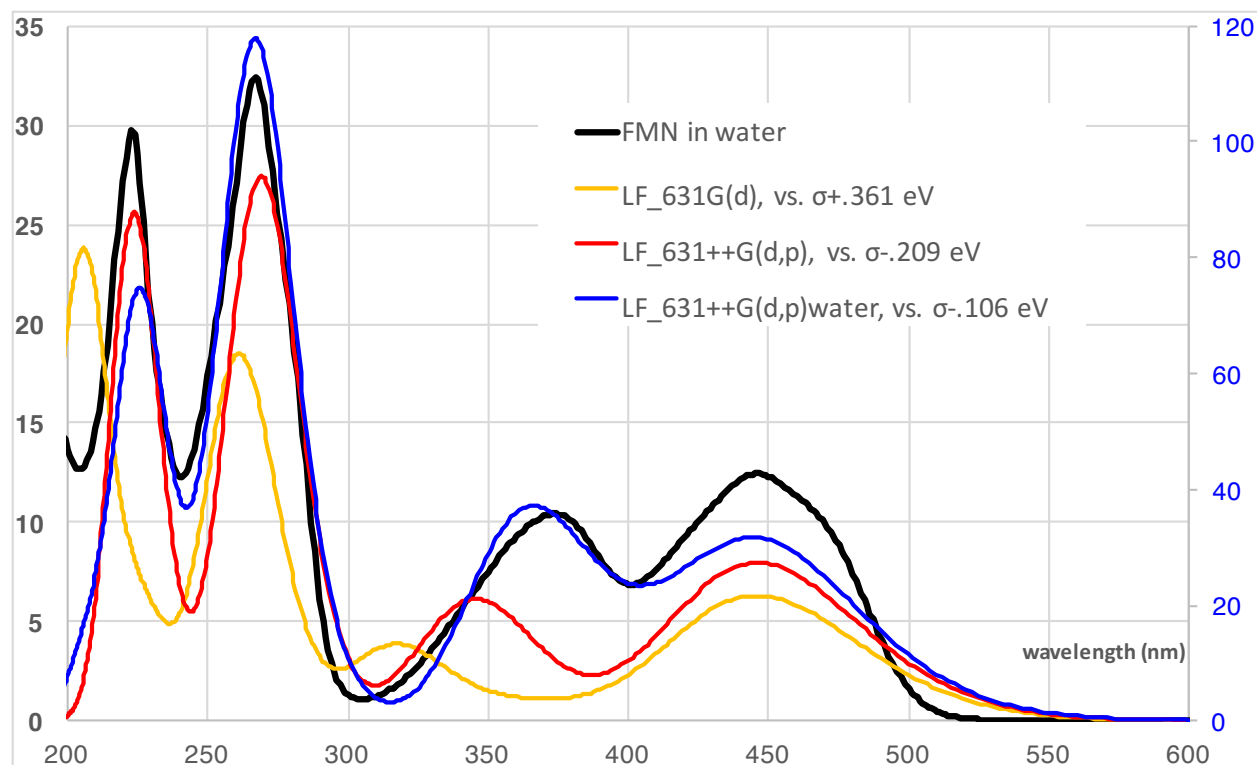


Figure S9: Comparison of the predictions made by different commonly-used basis sets, plotted with the experimental spectrum of FMN in water (black). The model calculations treated lumiflavin, in which the ribose is truncated at the C attached to the flavin. While the smaller basis set fails to reproduce the relative amplitudes of the two lowest-energy bands, the larger basis set does much better and its deficiency can be attributed to the in-vacuo treatment, although embedding the lumiflavin model in simulated water (continuous polarizable dipole field with the dielectric of water) appears to permit too large a polarization of the lumiflavin model.

Supplemental Figure S10

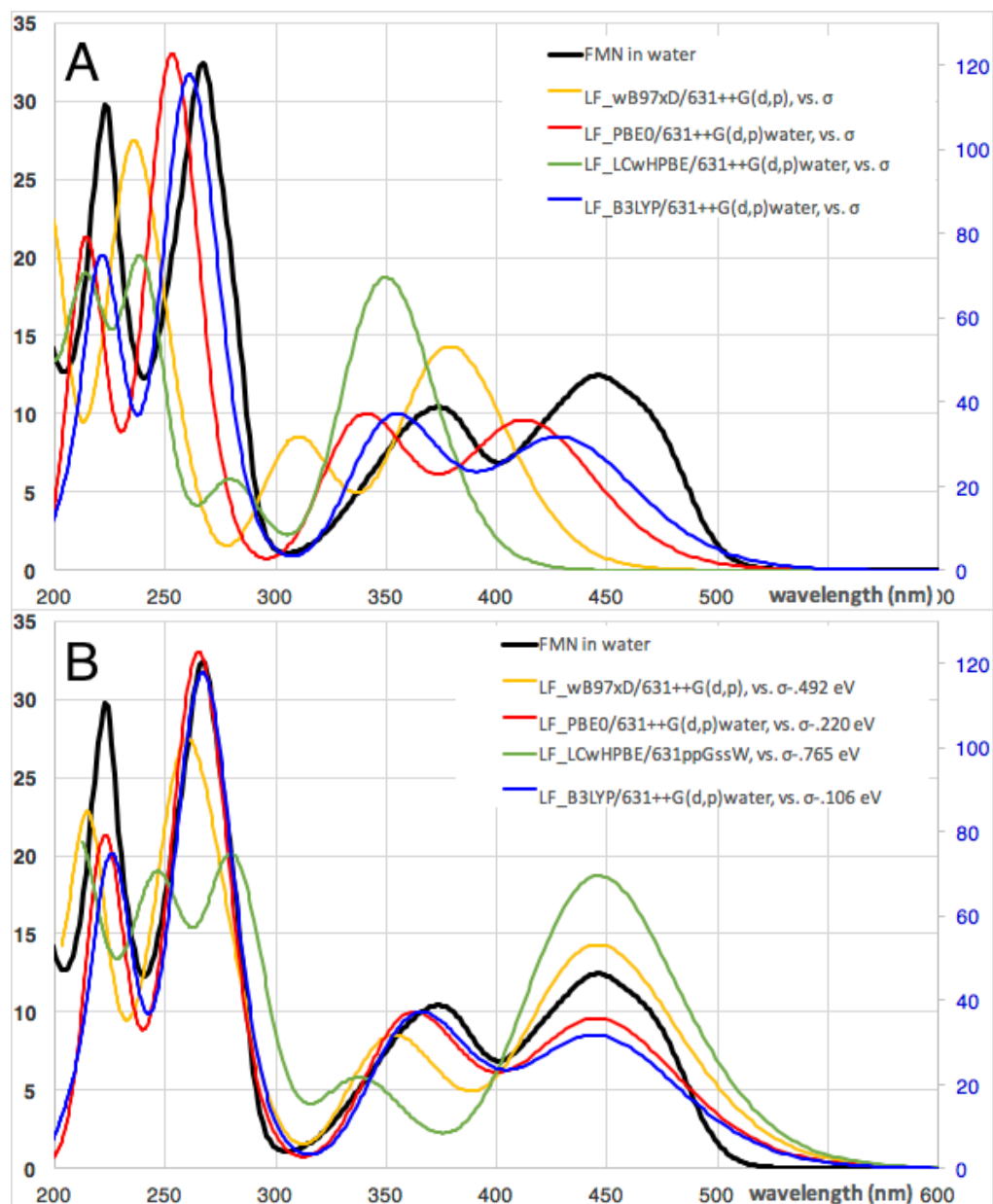


Figure S10: Comparison of the predictions made by four different commonly-used functionals, plotted with the experimental spectrum of FMN in water (black). In Panel A, no correction has been made to the excitation energies, so as to show which functionals do best in this regard (B3-LYP). In panel B, each prediction is plotted vs. an energy scale offset to produce the best agreement with experiment at 450 nm (conversion to nm was made after correction of energy in eV). This permits comparison with experiment of the relative strengths of the two lowest-energy bands, revealing PBE0 and B3LYP as the best choices and comparable to one-another.